L-shell ionization of selected medium-Z elements by 0.22–0.83-MeV u^{-1} carbon ions

I. Bogdanović, S. Fazinić,* and M. Jakšić
R. Bošković Institute, P.O. Box 1016, 10000 Zagreb, Croatia

Ž. Šmit
J. Stefan Institute, Ljubljana, Slovenia

(Received 18 February 1997)

Individual L-shell x-ray production cross sections were measured with ^{12}C ions in the energy range 0.22–0.83 MeV u^{-1} on Cd, In, Sb, Te, Ba, Tb, and Yb targets. From these measurements the L-subshell ionization cross sections were extracted and compared with the predictions of the direct ionization theories, i.e., with perturbed stationary state theory with energy loss, Coulomb deflection and relativistic corrections, the semiclassical approximation (SCA) in the united-atom limit, and SCA coupled-channel calculations involving a few lowest lying states. Better overall agreement between experiment and theory was found for the SCA theory. Inclusion of the SCA coupled-channel calculations improved the agreement for the L_2-subshell in the very adiabatic region, but theory fails to describe L_1-ionization cross sections, especially in the $0.4 < \xi_{L_1} < 0.7$ region. The degree of multiple ionization of outer shells caused by C ion bombardment was estimated from the x-ray line energy shifts and by comparing the x-ray intensity ratios for carbon ions and protons. [S1050-2947(97)02110-0]

PACS number(s): 34.50.Fa

I. INTRODUCTION

Inner-shell ionization induced by charged particle impact has been the subject of extensive experimental and theoretical investigations during the last few decades. Most of the experimental work published so far has been concentrated on the ionization of K and L shells by protons and α particles. The accumulated experimental data have been summarized in compilation works by several authors [1–4]. This interest is due to the fact that inner-shell ionization is of great importance in the development of different kinds of applications, like particle induced x-ray emission (PIXE), calculations of stopping power, ion implantation, and the study of solids and plasmas.

For the published data of K- and L-shell x-ray cross sections induced by ions heavier than α particles, the situation is quite different. In the works published so far, the data are very scanty concerning the studied elements, energy intervals, and projectiles, particularly for L-shell ionization. Very often, authors have reported only the total L-shell x-ray production cross sections, which is probably due to the very low x-ray production rate and the reduced resolving ability of Si(Li) x-ray detectors. Some of the experimental limitations of x-ray cross section measurements have been alleviated with the improved energy resolution of Si(Li) detectors (135 eV at 5.9 keV), or by the use of high resolution crystal spectrometers.

A limited number of studies exist of L-shell ionization by carbon ions [5–13]. Li *et al.* [5] studied L-shell ionization on Ta, Au, Bi, and U targets in the energy range from 0.5 to 8 MeV u^{-1}. Au was studied very often. For example, Sarkadi and Mukoyama [6] reported Au L_i-subshell ionization cross sections in the energy range 0.03–0.28 MeV u^{-1}, while Jitschin *et al.* [7] measured the same by 0.23–6.7 MeV u^{-1} ions. Mahli and Gray [9] reported individual $L\alpha_{1,2}$, $L\gamma_1$, and $L\gamma_{2,3,(6)}$ x-ray production cross sections of Yb and Au for energies from 0.5 to 3 MeV u^{-1}. Mehta *et al.* [13] reported the total L-shell x-ray production cross sections for selected elements between Cu and Pb in the energy range 0.17–1 MeV u^{-1}, Bhattacharya *et al.* [10] measured the individual L-subshell production cross sections for Au and Bi by 0.3–0.79 MeV u^{-1} C ions, and Braziewicz *et al.* [11] reported L_i-ionization cross sections for some rare earth elements with 0.4–2.8 MeV u^{-1} ions. Recently, Semaniak *et al.* [12] published the subshell ionization cross sections for some selected heavy elements with $72 \leqslant Z_2 \leqslant 90$ by carbon ions of energy 0.4–1.8 MeV u^{-1}.

The L shell presents a particularly sensitive ground for testing direct ionization theories because it consists of three subshells, all with different properties. Simultaneously with the experimental measurements, different theoretical models, such as the plane wave Born approximation (PWBA) [14], and the semiclassical approximation (SCA) [15,16], have been developed. The observed disagreement between experimental results and theoretical predictions has provoked further theoretical study and modification of the original PWBA theory to the more advanced ECPSSR theory [17,18]. The ECPSSR theory is the perturbed stationary state (PSS) theory adopted to account for projectile energy loss (E) and the Coulomb deflection (C) in the field of the target nucleus, and relativistic corrections (R) for describing the inner-shell electrons.

Both the ECPSSR and SCA theory proved to be adequate for description of K-shell ionization by protons and helium

*Present address: IAEA, Wagramerstrasse 5, A-1400 Vienna, Austria.

 © 1997 The American Physical Society

ions. However, in the case of L-shell ionization, even for protons, deviations from theory have been observed in the low ion velocity range [19,20]. As can be expected, these discrepancies are more pronounced for heavier projectiles. Vigilante *et al.* [20] showed that improvements can be achieved in the ECPSSR theory by modifying the binding correction factor. However, these corrections were not sufficient to explain the remaining disagreement between experiment and theory, especially for the L_2 subshell. Sarkadi and Mukoyama [21] suggested that the mechanism of vacancy sharing among subshells might be the cause of these differences. The main idea of this model is that a vacancy produced by direct ionization in one of the L subshells may be transferred to another subshell, and the result is the redistribution of vacancies between the subshells. Vigilante *et al.* [20] introduced this effect in the ECPSSR framework by using a simple two step model developed by Sarkadi and Mukoyama [22], and showed that this correction slightly improves the agreement between experiment and theory. Shingal *et al.* [23] used the coupled-channel semiclassical impact parameter model in conjunction with the independent electron model and target centered atomic orbital expansion to calculate the L_1-subshell ionization cross section. Their calculation showed improvement in the agreement between theory and experimental data. Recently, Sarkar *et al.* [24] compared the available experimental data for the L-subshell ionization induced by heavy ions with the predictions of the ECPSSR theory with and without intrashell coupling (IS). They included the IS correction factors calculated in the first-order approximation and neglected the interference terms as suggested by Sarkadi and Mukoyama [25]. The result of this inclusion was a substantially improved agreement between experiment and theory for the L_2 subshell, but without essential difference in the analysis of L_1- and L_3-subshell data. Smit and Orlić [26] made a comparison between the experimentally determined proton induced L_i-subshell ionization cross sections and theory calculated by the coupled-channel method and by the first-order SCA-UA (UA denotes united atom). The result of their investigations was that the inclusion of the IS coupling effect improves the agreement between experiment and theory except in the very adiabatic region, where the experimental data are scanty and uncertain. Sarkadi *et al.* [27] made coupled-state calculations for the ionization of the Au and Bi L subshells by B ions in the energy range 0.48–0.88 MeV u^{-1} and compared their results with the experimental data reported by Padhi *et al.* [28]. They found satisfactory agreement between the experimental data and the coupled-states model. Also they reported that the agreement between the experimental data and the coupled-channel model developed by Šmit and Orlić [26] is better for the L_1 and L_2 subshells, but for the L_3 subshell, the experimental points are closer to the coupled-states model of Sarkadi [29].

In the present paper we report the individual L shell x-ray production cross sections for $L\alpha_{1,2}$, $L\beta_{1,3,4}$, $L\beta_{2,15}$, $L\gamma_{15}$, and $L\gamma_{2,3(4,4')}$ x-ray lines and the corresponding L_1-, L_2-, and L_3-subshell ionization cross sections for Cd, In, Sb, Te, Ba, Tb, and Yb measured with ^{12}C ions in the energy range from 0.22 to 0.83 MeV u^{-1}. The results are compared with the predictions of the ECPSSR theory and SCA calculations of Šmit and Orlić [26] in the UA limit and in the few-state coupled-channel model.

II. EXPERIMENT

All the measurements were performed with ^{12}C ions in the energy range from 0.22 to 0.83 MeV u^{-1}, using the EN tandem Van de Graaff accelerator at the Ruder Bošković Institute, Zagreb. The trajectory of the incident beam was defined by a set of four collimator slits which gave a 2 mm diameter beam spot on the target. All targets used were 20 μg cm^{-2} thick, deposited on 20 μg cm^{-2} thin carbon foil (Micromatter, USA). The L-shell x-ray spectra were collected by a Si(Li) detector (Link Analytical) with a nominal active area of 80 mm^2, a Be window of 12.5 μm, and a measured full width at half maximum (FWHM) of 150 eV at 5.9 keV. The detector was mounted inside the vacuum chamber at 135° to the beam axis. Thick molybdenum foil with a 7 mm diameter aperture was placed in front of the detector to reduce the low energy tailing induced by incomplete charge collection arising from edge effects. The aperture was covered with a 55 μm thick Kapton foil to attenuate the intense M-shell x rays. Together with the L-shell x-ray lines, the spectra of backscattered ions were collected using an annular silicon surface-barrier (SB) detector with an area of 400 mm^2, positioned at a mean angle of 171° to the beam axis. The relative Si(Li) detector efficiency was determined using the procedure described by Pajek *et al.* [30]. K-shell x rays from a set of thin calibration targets of light elements ($13 < Z_2 < 39$) were produced by 1.8 MeV protons and measured with the Si(Li) detector in the same configuration as was used for the L-shell x-ray measurements. At the same time, the backscattered protons were measured by the SB detector at the same geometry. The K-shell theoretical ECPSSR ionization cross sections corrected for Paul's empirical factor [1], as calculated by the TTPIXAN [31] computer code, were used for the efficiency calibration. In the region of interest (3–11 keV), the measured efficiency had an uncertainty between 6% and 9% for higher and lower energies, respectively, because the uncertainties of the fluorescence yields [32] for $Z_2 < 20$ are higher. For absolute efficiency normalization, an ^{55}Fe radioactive source was used.

The nonlinear least-squares fitting routine AXIL [33] was used for background subtraction from the x-ray spectra and for extracting the Ll, $L\alpha_{1,2}$, $L\beta_{1,3,4}$, $L\beta_{2,15}$, $L\gamma_{1,5}$, and $L\gamma_{2,3(4,4')}$ x-ray intensities. For some lines more than one Gaussian was used to fit the individual x-ray transitions, mainly because of the broadening of x-ray lines due to the outer-shell multiple ionization occurring in the heavy ion collision. Individual L-shell x-ray production cross sections $\sigma^x_{L_i}$ were calculated by normalization of the x-ray intensities to the corresponding ion backscattering intensities, using the following equation:

$$\sigma^x_{L_i} = \frac{4\pi Y_x \sigma_i \Omega_i}{Y_i \epsilon_i \Omega_x} F(E, \Delta E), \tag{1}$$

where Y_x and Y_i are the x-ray and the backscattered ion intensities corrected for dead time, Ω_x and Ω_i are the x-ray and particle detector solid angles, σ_i is the differential back-

scattering cross section (b/sr), ϵ_i is the x-ray detector efficiency, and $F(E,\Delta E)$ is the correction factor due to ion energy loss and self-absorption of outgoing x rays inside the target.

Assuming that the x-ray production cross section $\sigma^x_{Li}(E)$ and the stopping power $S(E)$ are proportional to E^α and E^β, respectively, near the ion energy E_0, the correction factor $F(E,\Delta E)$ can be written as [11]

$$F(E,\Delta E)=\frac{1+\frac{1}{2}(2+\beta)(\Delta E/E_0)+\frac{1}{6}(2+\beta)(3+\beta)(\Delta E/E_0)^2}{1-\frac{1}{2}(\alpha-\beta+\mu\overline{x})(\Delta E/E_0)+\frac{1}{6}[(\alpha-\beta)(\alpha-\beta-1)+(2\alpha-3\beta)\mu\overline{x}+(\mu\overline{x})^2](\Delta E/E_0)^2}, \tag{2}$$

where μ is the x-ray mass attenuation coefficient calculated from the data of Thin and Leroux [34], $\overline{x}=[E/S(E)]/(\cos\gamma/\cos\delta)$, with γ being the angle between the target normal and the beam axis, and δ is the angle between the target normal and the direction towards the x-ray detector. These two angles were 0° and 45°, respectively. The stopping power $S(E)$ and the coefficient β were calculated from the data of Ziegler *et al.* [35], while the coefficient α was determined iteratively from the measured data points using Eq. (1). A few iterations were necessary, with the initial guess $F(E,\Delta E)=1$. In our case, $F(E,\Delta E)$ exceeded unity by less than 8% for all targets and energies used in the measurements. The total experimental uncertainties of the measured x-ray production cross sections are summarized in Table I.

The scattering cross section σ_i can deviate from its Rutherford value for two main reasons: the screening effects due to the surrounding electrons at lower ion energies, and nuclear-force interactions between the projectile and target nucleus at higher ion energies. According to the model developed by Bozoian *et al.* [36], the nuclear-force interactions between the projectile and target nucleus contribute to the scattering cross section at energies which are much higher than those used in the present measurements. So, we used the Rutherford backscattering cross sections with the screening effect included according to L'Ecuyer *et al.* [37]. This effect was highest for the Yb target bombarded by 2.6 MeV ions (3%).

The L-subshell ionization cross sections σ_{L_1}, σ_{L_2}, and σ_{L_3} were calculated from the measured $\sigma_{L\alpha_{1,2}}$, $\sigma_{L\gamma_{1,5}}$ and $\sigma_{L\gamma_{2,3(4,4')}}$ x-ray production cross sections using the following relations:

$$\sigma_{L_1}=\frac{\sigma_{L\gamma_{2,3(4,4')}}\Gamma_{L_1}}{\omega_{L_1}\Gamma_{\gamma_{2,3(4,4')}}}, \tag{3}$$

TABLE I. Total experimental uncertainties of the measured x-ray production cross sections with carbon ions.

Z	$L\alpha_{1,2}$	$L\beta_{1,3,4}$	$L\beta_{2,15}$	$L\gamma_{1,5}$	$L\gamma_{2,3(4,4')}$
Cd	11	11	11	12	13
In	10	10	10	12	13
Sb	11	10	10	11	12
Te	10	10	10	12	13
Ba	10	10	10	11	13
Tb	10	10	10	12	14
Yb	10	10	10	12	14

$$\sigma_{L_2}=\frac{\sigma_{L\gamma_{1,5}}\Gamma_{L_2}}{\omega_{L_2}\Gamma_{\gamma_{1,5}}}-\sigma_{L_1}f_{12}, \tag{4}$$

$$\sigma_{L_3}=\frac{\sigma_{L\alpha_{1,2}}\Gamma_{L_3}}{\omega_{L_3}\Gamma_{\alpha_{1,2}}}-\sigma_{L_1}(f_{12}f_{23}+f_{31})-\sigma_{L_2}f_{23}, \tag{5}$$

where $\Gamma_{\gamma,\alpha}$ and Γ_{L_i} are the individual and total radiative widths taken from Campbell and Wang [38]; ω_i and f_{ij} are the single hole fluorescence and Coster-Kronig transition yields taken from Chen *et al.* [39].

III. RESULTS AND DISCUSSION

The individual L-shell x-ray production cross sections for the investigated elements measured with ^{12}C ions are summarized in Table II. Only a few experimental data exist for comparison with the present measurements. For Yb, there are two sets of measurements with carbon ions. Mehta *et al.* [13] reported the total L-shell x-ray production cross sections at 8 and 10 MeV. Their result at 8 MeV is 50% lower, and at 10 MeV 30% lower than ours. Mahli and Gray [9] measured the individual $L\alpha_{1,2}$, $L\gamma_1$ and $L\gamma_{2,3,(6)}$ x-ray production cross sections in the energy range from 0.5 to 3 MeV. Their data are compared with our results and with the predictions of the ECPSSR theory in Fig. 1. For all other elements measured with C ions and reported in the present work, as far as the authors know, no experimental data have been published.

In Fig. 2, the ratios between the experimental L_i-ionization cross sections and the predictions of the ECPSSR theory ($\sigma_{\rm expt}/\sigma_{\rm ECPSSR}$) are presented as a function of the reduced velocity parameter $\xi_{L_i}=2v_1/\theta_{L_i}v_{L_i}$, where v_1 is the projectile velocity and v_{L_i} is the electron velocity in the L_i subshell. The parameter θ_{L_i} is the reduced electron binding energy defined as $\theta_{L_i}=n^2U_{2L_i}/Z^2_{2L_i}\mathcal{R}$, where n is the principal quantum number, U_{2L_i} is the experimental binding energy of the target atom electron, $Z_{2L_i}=Z_2-4.15$ is the screened nuclear charge according to the recipe of Slater, and $\mathcal{R}$ is the Rydberg constant. As can be seen from Fig. 2, large deviations from the ECPSSR theory exist for all three subshells. For the L_1 subshell, the experimental data are systematically higher than the predictions of the ECPSSR theory for $\xi>0.5$. This ratio reaches a maximum at $\xi\approx 0.7$ for all the elements, except for Cd and In. In the case of these two elements the limited resolution of the Si(Li) detector imposes difficulties in extracting the L_1-ionization cross sec-

TABLE II. Individual L-shell x-ray production cross sections (b) measured with ^{12}C ions.

Z	E (keV)	$L\alpha_{1,2}$	$L\beta_{1,3,4}$	$L\beta_{2,15}$	$L\gamma_{1,5}$	$L\gamma_{2,3(4,4')}$
Cd	2600	52.60	27.30	5.16	2.00	0.98
	3400	119.00	59.30	11.90	4.90	1.75
	4200	206.00	98.90	23.40	7.69	2.98
	5000	319.80	150.80	37.10	12.60	4.69
	6000	488.60	226.40	57.50	22.60	7.01
	8000	980.10	443.20	126.20	48.90	17.00
	9000	1316.50	608.90	156.20	59.60	25.30
	10000	1708.70	801.80	215.50	76.20	35.20
In	5000	278.70	119.40	23.40	10.20	2.75
	5300	316.00	134.80	29.60	14.50	4.73
	5900	419.00	176.70	40.80	21.10	6.72
	6400	535.70	218.00	52.00	26.90	8.26
	7000	664.70	264.60	65.50	32.80	9.79
	7600	860.50	350.00	87.90	41.20	14.10
	8200	958.40	385.70	99.50	46.90	16.90
	8800	1059.90	444.60	117.00	55.90	20.20
	9400	1743.80	700.90	181.20	85.60	32.30
	10000	2426.60	1021.10	276.20	104.80	51.00
Sb	2600	28.60	15.20	2.73	1.29	0.51
	3400	73.50	34.90	8.36	2.82	1.12
	4200	130.20	60.00	15.10	5.33	1.99
	5000	210.70	97.30	25.10	8.83	2.99
	6000	311.20	138.40	38.40	14.20	4.91
	7000	423.30	182.20	55.70	18.10	6.95
	8000	523.50	224.90	72.10	23.60	9.25
	9000	968.50	410.10	137.40	45.60	17.80
	10000	1255.40	531.50	180.90	60.60	25.60
Te	3400	59.10	28.10	6.58	3.18	0.79
	4200	110.90	52.80	11.80	6.19	1.37
	5000	167.70	79.70	18.00	9.20	2.16
	6000	265.60	120.20	32.10	11.90	4.36
	7000	365.20	161.80	44.80	16.10	5.90
	8000	470.60	206.20	60.20	22.80	7.52
	9000	737.70	319.80	97.40	35.90	12.80
	10000	988.20	432.90	129.70	48.60	20.30
Ba	2600	10.20	5.86	1.25	0.55	0.19
	3400	30.40	15.10	3.93	1.47	0.53
	4200	58.80	27.60	7.64	2.84	1.07
	5000	94.40	42.90	12.20	4.28	1.60
	6000	151.10	68.20	20.40	6.87	2.99
	7000	220.70	96.10	30.40	10.00	4.20
	8000	298.90	128.00	42.60	13.40	6.00
	9000	440.10	181.60	65.70	21.00	8.04
	10000	567.20	231.80	85.60	29.20	9.86
Tb	3400	6.58	4.03	0.96	0.56	0.15
	4200	15.30	8.36	2.37	1.15	0.30
	5000	27.60	13.90	4.38	2.06	0.46
	6000	47.40	22.50	7.65	3.33	0.76
	7000	73.80	33.90	12.00	5.04	1.24
	8000	104.00	44.40	17.90	7.00	1.60
	9000	140.10	58.40	24.30	9.23	2.20
	10000	184.40	75.60	32.30	11.90	2.97
Yb	6000	25.60	12.40	4.45	1.94	0.53
	7000	41.60	19.20	7.29	2.99	0.80
	8000	59.40	26.00	10.90	4.22	1.14
	9000	79.00	33.90	14.70	5.21	1.51
	10000	107.80	45.50	19.90	6.84	2.06

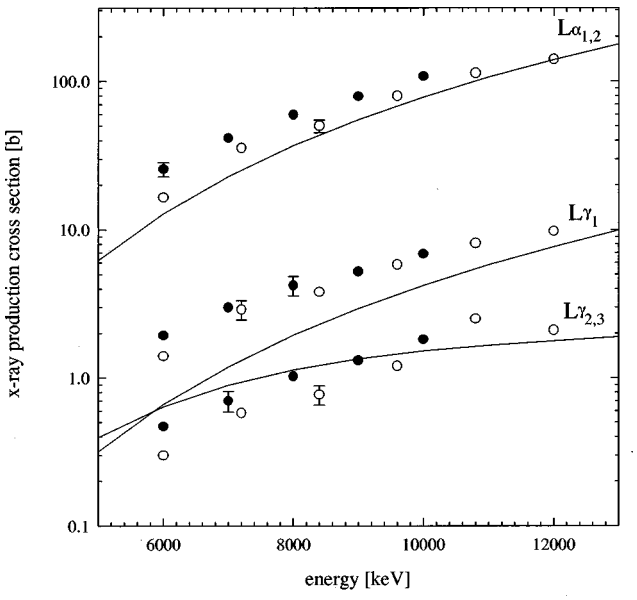

FIG. 1. $L\alpha_{1,2}$, $L\gamma_1$, and $L\gamma_{2,3}$ x-ray production cross sections for a Yb target bombarded by carbon ions (open circles–Mahli and Gray [9], closed circles–present measurements, lines–predictions of the direct ionization ECPSSR theory). Typical error bars are shown.

tions from the weakest $L\gamma_{2,3}$ lines. The x-ray spectra are also broadened due to multiple outer-shell ionization. For L_2 and L_3 subshells at the lowest velocities, the cross section ratio ($\sigma_{\text{expt}}/\sigma_{\text{ECPSSR}}$) reaches a factor of about 5, and then gradually decreases for higher velocities. A similar tendency was reported by Braziewicz *et al.* [11] for the case of some rare earth elements bombarded by carbon ions, and Semaniak *et al.* [12] for some heavier elements ($Z>72$). The data from Ref. [12] are compared with ours in Fig. 2. It was already pointed out by some authors [11,20,40] that the binding correction used in the ECPSSR theory leads to an overestimation of the effective binding energy in the low energy limit when it is calculated using undistorted screened hydrogenic wave functions. Some modifications of the ECPSSR binding correction were proposed [11,20] which moved theory closer to experiment, though not decisively.

As we compared our results only with the predictions of the direct ionization ECPSSR theory, it is necessary to estimate the possible electron capture (EC) contribution to the cross section. For the present measurements, the incoming C ions without K-shell vacancies were used, but an EC contribution can arise due to the finite target thickness [41]. The relevant parameter to consider is the ratio between the projectile K-shell and target L-subshell binding energies of interest. In our case, this ratio is lower than 0.1 for all targets. Gardner *et al.* [43] observed for similar K binding energy ratios in the case of F ions on Cu targets that the EC contribution was less than 10%. Experimentally, x-ray production cross sections as a function of target thickness have already been studied by many authors [11,13,41,42]. Schiebel *et al.* [42] measured Ag L x-ray yields as a function of target thickness (2–40 μg cm^{-2}) from 10–40 MeV F ions with charge states 6^+ to 9^+. They found that for 6^+ ions the x-ray yield was independent of target thickness. Sun *et al.* [41] measured M-shell x-ray production cross sections with

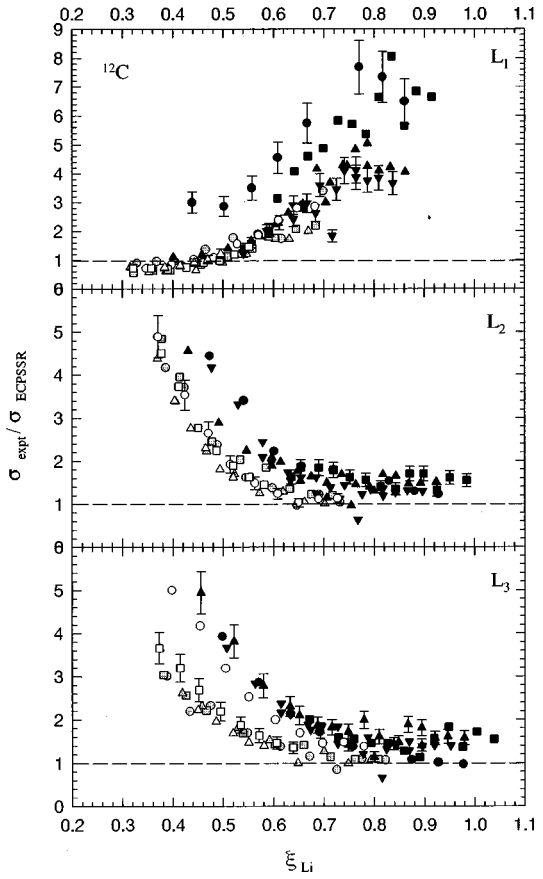

FIG. 2. Ratio of the experimental L-subshell ionization cross sections and the direct ionization ECPSSR theoretical predictions for ^{12}C ions, as a function of the scaled velocity ξ_{L_i}. Symbols used are the following: (a) present measurements: Cd–black circles; In – black squares; Sb–black triangles; Te–inverted black triangles; Ba–white circles; Tb–white squares; Yb–white triangles; (b) data from Ref. [12]: Hf–gray circles; Ta–gray squares; W–gray triangles. Typical error bars are shown.

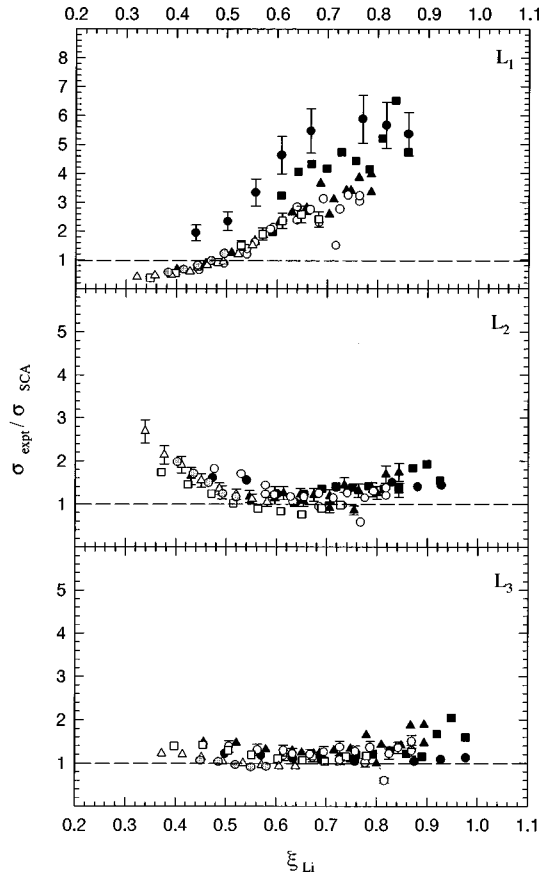

FIG. 3. Ratio of the experimental L-subshell ionization cross sections and the SCA-UA theoretical predictions [26] for ^{12}C ions as a function of the scaled velocity ξ_{L_i}. Symbols used are the following: Cd–black circles; In–black squares; Sb–black triangles; Te–white circles; Ba–white squares; Tb–white triangles; Yb–gray triangles. Typical error bars are shown.

8 MeV ^{12}C ions on Ho as a function of the target thickness. They found that for targets thicker than 14 μg cm^{-2}, independently of the ion charge state, the x-ray production cross section becomes constant. They also reported that the cross section difference between thin targets and the charge-state equilibrium targets was about 10% for incoming 8 MeV ^{12}C ions without K-shell vacancies. Braziewicz *et al.* [11] examined the L-shell ionization of La and Dy targets with different thicknesses (1–250 μg cm^{-2}) by $^{12}C^{+4,+5,+6}$ ions of 26.4 MeV energy. They found that for targets thicker than 15 μg cm^{-2}, the L x-ray production was practically independent of the target thickness and projectile charge state. As our targets were 20 μg cm^{-2} thick, and C ions with charge states $q=+2,+3$ were used, we assume that the L-shell x-ray cross sections reported here are equilibrium cross sections and that the EC contribution cannot be higher than a few percent.

Better overall agreement was found between the experimental data and the predictions of the SCA theory. Data were compared with the SCA theory [26] in the united-atom limit (Fig. 3) which was improved further by including correction factors from a simple coupled-channel model (Fig. 4). In the united-atom approximation, the electron binding energies and the wave functions are essentially those of a virtual atom with the atomic number $Z_1 + Z_2$. This is justified for sufficiently slow collisions, characterized by a reduced velocity parameter ξ smaller than unity. In the SCA approach [26], the projectile motion is assumed to follow a classical hyperbolic trajectory, and the atomic electrons are described by screened hydrogenic wave functions. The screening due to inner electrons was taken into account according to Slater, and that due to outer electrons according to Bethe.

The differences between the experimental data and the SCA theory are largest for the L_1 subshell at the highest ion velocities. Good agreement was found for the L_3 subshell, where the differences between experiment and theory are generally lower than 40% for the entire energy range. For the L_2 subshell, the agreement between experiment and SCA theory is better, and typical cross section differences in the very adiabatic region are reduced to a factor of 2. For the L_1 subshell and the lowest energies investigated, the experimental data are lower by up to 60% than the theoretical predictions. Around $\xi \approx 0.5$, the experimental data start to be systematically larger than the theoretical predictions, and exceed them by a factor of 3 at the highest energies investigated.

The subshell coupling effects, in the few-state coupled-

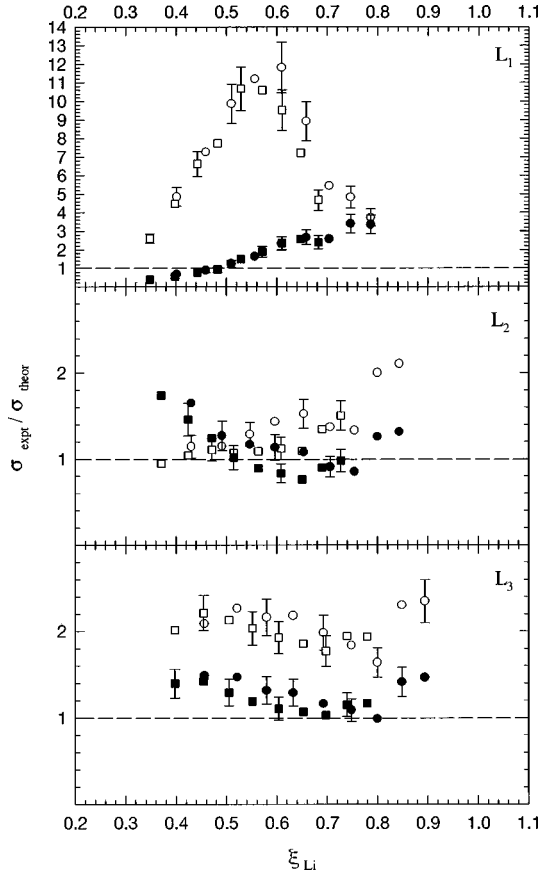

FIG. 4. Measured L-shell ionization cross sections normalized to (a) first order SCA-UA predictions (full symbols), (b) few-state SCA coupled-channel calculations (hollow symbols) [26]. Circles are for an Sb target and squares for a Ba target bombarded with ^{12}C ions. Typical error bars are shown.

channel model of Šmit and Orlić [26], were calculated for Sb and Ba in the form of correction factors, given as the cross section ratios $\sigma_{L_i}^{\mathrm{CC}} / \sigma_{L_i}^{\mathrm{UA}}$. Here $\sigma_{L_i}^{\mathrm{CC}}$ was obtained by solving a system of coupled equations, and $\sigma_{L_i}^{\mathrm{UA}}$ was calculated in the first-order approximation and in the united-atom limit [26]. The model [26] simultaneously accounts for the redistribution of vacancies and the binding effect. Due to the small number of states involved in the calculation (eight bound and a virtually bound $4s,p$ state representing the continuum), the calculated cross sections may be too low, mainly due to the overestimated binding effect. Figure 4 indicates that the inclusion of the intrashell coupling effect improves the agreement between theory and experiment for the L_2 subshell in the low energy region. For the L_3 subshell, the coupled-channel calculations predict slightly higher cross section ratios than the SCA-UA. For the L_1 subshell, the cross section differences become significant, especially for the $0.4 < \xi_{L_1} < 0.7$ region where they reach a factor of 12 for $\xi \approx 0.6$. Similar general behavior (improvement for L_2, no role in the analysis of L_3, and somewhat worse agreement with experiment for the L_1 subshell) was already reported by Sarkar *et al.* [24]. They compared the ECPSSR theory with and without intrashell coupling for different heavy ion-target combinations. The same was done by Sarkadi *et al.* [27] in the case of B bombardment on Au and Bi. In both works [26,27], only the $\xi_{L_1} < 0.42$ region was investigated, and the significant deficiency of the coupled-channel model as found in the present study in the $0.4 < \xi_{L_1} < 0.7$ region was not detected. Several approximations which were used for developing the coupled-channel model [26] may be responsible for the effect. The choice of nonrelativistic hydrogenic wave function for the L_1 subshell may be critical due to its nodal structure. However, the most important limitation of the model [26] is the small number of states included, which are unable to reproduce the collisionally induced evolution of atomic wave functions. The number of states required for the calculation would then increase with the size of the perturbation, i.e., with the Z_1/Z_2 ratio. The differences between the calculated [26] and experimental cross sections are therefore larger for larger Z_1/Z_2 ratios. For the L_1 subshell, the importance of proper wave function expansion was already demonstrated in [23].

For conversion of the x-ray production cross sections into ionization cross sections we used single hole fluorescence and Coster-Kronig transition yields. It is well known that for heavy ions the probability of producing more than one vacancy during a collision cannot be neglected. Therefore it is important to estimate the influence of multiple ionization on the atomic parameters. The presence of spectator vacancies in the M and higher shells during the L-shell vacancy decay causes an energy shift of the L x rays. The relative intensities of x-ray lines filling the same L subshell vacancy may also vary. Thus both the x-ray shifts and the relative intensities can give information about the degree of outer-shell multiple ionization during x-ray emission. Fortner *et al.* [44] calculated the variations of the L-shell fluorescence yield in copper as a function of the M-shell vacancy number. They found that the copper L-shell fluorescence yield is essentially constant (varies less than 10%) for as many as six M-shell vacancies. For elements with a full M shell in the ground state, the removal of the first few $3d$ electrons changes the x-ray and Auger transition rates by the same proportion, and the fluorescence yield remains relatively unchanged. To estimate the degree of multiple ionization, the HF86 [45] general Hartre-Fock program was used for calculating the $L\alpha_{1,2}$ ($M_{4,5}$-L_3) and $L\beta_{2,15}$($N_{4,5}$-L_3) transition energies for different numbers of spectator M vacancies. The N-shell vacancies were not included in the calculations, since the energy shifts caused by N vacancies are more than one order of magnitude lower than those caused by M vacancies. The number of M-shell vacancies V_M was estimated separately for $L\alpha_{1,2}$ and $L\beta_{2,15}$ x-ray lines by comparing the experimental (ΔE_{expt}) and calculated [45] energy shifts. As can be seen from Table III, the results for V_M obtained from the two x-ray lines at the same impact energy are in good agreement. However, the results obtained from $L\beta_{2,15}$ are more reliable, since the energy shifts for $L\alpha_{1,2}$ in the case of Tb are close to the experimental uncertainties of the x-ray energy determination, which was estimated to be 8 eV. It can also be concluded that the degree of M-shell ionization slightly increases with ion energy, and is higher for lower Z_2 targets. The degree of multiple ionization for the N shell (V_N) was calculated by comparing the measured and theoretical Dirac-Hartree-Fock x-ray line intensity ratios [38] and by using the statistical scaling procedure of Larkins [46]. According to [46], the x-ray intensity ratio $(I(L\alpha_{1,2})/I(L\beta_{2,15}))_C$ in the

TABLE III. Average number of M-shell vacancies (V_M) calculated from the $L\alpha_{1,2}$ and $L\beta_{2,15}$ x-ray energy shifts (ΔE_{expt}) for 3.4 and 10 MeV carbon ions. The average number of N-shell vacancies (V_N) was estimated by comparing the $I(L\alpha_{1,2})/I(L\beta_{2,15})$ x-ray intensity ratios obtained by carbon ion bombardment with the theoretical values of Campbell and Wang [38] and using the statistical scaling procedure of Larkins [46]. After V_N was determined, V_O was estimated applying a similar procedure for the $I(L\gamma_{2,3})/I(L\gamma_{4,4'})$ ratio.

Z	Energy (MeV)	X ray	ΔE_{expt} (eV)	V_M	$(I(L\alpha_{1,2})/I(L\beta_{2,15}))_C$	$(I(L\gamma_{2,3})/I(L\gamma_{4,4'}))_C$	V_N	V_O
Ba	3.4	$L\alpha_{1,2}$	20	1.3				
	3.4	$L\beta_{2,15}$	71	1.5	7.74	5.80	3.5	3.4
	10.0	$L\alpha_{1,2}$	31	1.9				
	10.0	$L\beta_{2,15}$	89	1.9	6.63	6.84	2.8	3.3
Tb	3.4	$L\alpha_{1,2}$	12	0.8				
	3.4	$L\beta_{2,15}$	54	1.0	6.83	6.68	2.6	2.5
	10.0	$L\alpha_{1,2}$	15	0.9				
	10.0	$L\beta_{2,15}$	69	1.3	5.71	6.37	1.3	1.0

presence of additional vacancies in the M and N shells is given by

$$\left(\frac{I(L\alpha_{1,2})}{I(L\beta_{2,15})}\right)_C = \left(\frac{I(L\alpha_{1,2})}{I(L\beta_{2,15})}\right)_0 \frac{1-V_M/10}{1-V_N/10}, \qquad (6)$$

where $(I(L\alpha_{1,2})/I(L\beta_{2,15}))_0$ is the x-ray intensity ratio for an atom with no vacancies in the M and N shells, and V_M and V_N are the numbers of spectator vacancies in the two shells, respectively. The experimental line ratios for Ba and Tb at 3.4 and 10 MeV are given in Table III. From [38], the $(I(L\alpha_{1,2})/I(L\beta_{2,15}))_0$ theoretical x-ray intensity ratio is 5.86 for Ba and 5.59 for Tb. The degree of O-shell ionization was obtained by a similar scaling procedure, using the measured $I(L\gamma_{2,3})/I(L\gamma_{4,4'})$ intensity ratio and the vacancy number V_N estimated from Eq. (6). The theoretical $(I(L\gamma_{2,3})/I(L\gamma_{4,4'}))_0$ x-ray intensity ratio is 5.98 for Ba and 7.01 for Tb [38]. The calculated number of V_N and V_O vacancies is shown in Table III. Concerning the estimated degree of outer-shell ionization for Ba and Tb in the investigated energy range, and following the argumentation given in [44], we can conclude that the variation of the fluorescence yield caused by multiple outer-shell ionization is only a few percent.

IV. CONCLUSION

The L-subshell ionization cross sections for selected elements $48 \leqslant Z \leqslant 70$ were measured by carbon ions in the energy range 0.22–0.83 MeV u^{-1}. The experimental data were compared with the predictions of direct ionization theories, i.e., the ECPSSR theory and the SCA theory in the united-atom approximation. A better agreement between the experimental data and theory was found for the SCA-UA theory, especially for L_2 and L_3 subshells, which is due to the inclusion of an appropriate binding correction for the adiabatic region. Inclusion of the intrashell coupled-channel calculations further improved the agreement between experiment and theory for the L_2 subshell in the very adiabatic region, but the theory fails to describe the behavior of the L_1 subshell in the $0.4 < \xi_{L_1} < 0.7$ region. Further theoretical studies are needed to explain this observation. The degree of outer-shell ionization was estimated from the x-ray energy shifts and variations of the x-ray intensity ratios for the two elements Ba and Tb. It can be concluded that this degree of outer shell ionization cannot influence L-subshell fluorescence yields by more than a few percent.

ACKNOWLEDGMENTS

The authors are indebted to Dr. Ivo Orlić from the National University of Singapore for providing Micromatter targets and to colleagues from the Laboratory for Nuclear Microanalysis, Zagreb, for their help in running the accelerator.

[1] H. Paul and J. Muhr, Phys. Rep. **135**, 47 (1986).
[2] H. Paul and J. Sacher, At. Data Nucl. Data Tables **42**, 105 (1989).
[3] R. S. Sokhi and D. Crumpton, At. Data Nucl. Data Tables **30**, 49 (1984).
[4] I. Orlić, C. H. Sow, and S. M. Tang, At. Data Nucl. Data Tables **56**, 159 (1994).
[5] T. K. Li, D. L. Clark, and W. Greenles, Phys. Rev. Lett. **37**, 1209 (1976).
[6] L. Sarkadi and T. Mukoyama, J. Phys. B **13**, 2255 (1983).
[7] W. Jitschin, R. Hippler, K. Finck, R. Schuch, and H. O. Lutz, J. Phys. B **16**, 4405 (1983).
[8] M. C. Andrews, F. D. McDaniel, J. L. Duggan, P. D. Miller, P. L. Pepmiller, H. F. Krause, T. M. Rosseel, L. A. Rayburn, R. Mehta, and G. Lapicki, Nucl. Instrum. Methods Phys. Res. B **10/11**, 181 (1985); Phys. Rev. A **36**, 3699 (1987).
[9] N. B. Mahli and T. J. Gray, Phys. Rev. A **44**, 7199 (1991).
[10] D. Bhattacharya, M. Sarkar, M. B. Chatterjee, P. Sen, G. Kuri,

D. P. Mahapatra, and G. Lapicki, Phys. Rev. A **49**, 4616 (1994).
[11] J. Braziewicz, J. Semaniak, T. Czyżewski, L. Glowacka, M. Jaskóla, M. Haller, R. Karschnick, W. Kretschmer, and D. Trautmann, J. Phys. B **27**, 1535 (1994).
[12] J. Semaniak, J. Braziewicz, M. Pajek, T. Czyżewski, L. Glowacka, M. Jaskóla, M. Haller, R. Karschnick, W. Kretschmer, Z. Halabuka, and D. Trautmann, Phys. Rev. A **52**, 1125 (1995).
[13] R. Mehta, H. L. Sun, D. K. Marble, J. L. Duggan, F. D. McDaniel, and G. Lapicki, J. Phys. B **28**, 1187 (1995).
[14] E. Merzbacher and L.W. Lewis, in *X-Ray Production by Heavy Charged Particles*, edited by S. Flugge, Encyclopedia of Physics Vol. 34 (Springer, Berlin, 1958).
[15] J. Bang and J. M. Hansteen, K. Dan. Vidensk. Selsk. Mat. Fys. Medd. **31**, 13 (1959).
[16] J. M. Hansteen and O. P. Mosebekk, Z. Phys. **234**, 281 (1970).
[17] W. Brandt and G. Lapicki, Phys. Rev. A **20**, 465 (1979).
[18] W. Brandt and G. Lapicki, Phys. Rev. A **23**, 1717 (1981).
[19] D. D. Cohen, Nucl. Instrum. Methods Phys. Res. **218**, 795 (1983).
[20] M. Vigilante, P. Cuzzocrea, N. De Cesare, F. Murolo, E. Perillo, and G. Spadaccini, Nucl. Instrum. Methods Phys. Res. B **51**, 232 (1990).
[21] L. Sarkadi and T. Mukoyama, J. Phys. B **14**, L225 (1981).
[22] L. Sarkadi and T. Mukoyama, Nucl. Instrum. Methods Phys. Res. B **4**, 296 (1984).
[23] R. Shingal, N. B. Malhi, and T. J. Gray, J. Phys. B **25**, 2055 (1992).
[24] M. Sarkar, D. Bhattacharya, M. B. Chatterjee, P. Sen, G. Kuri, D. P. Mahapatra, and G. Lapicki, Nucl. Instrum. Methods Phys. Res. B **103**, 23 (1995).
[25] L. Sarkadi and T. Mukoyama, Nucl. Instrum. Methods Phys. Res. B **61**, 167 (1991).
[26] Ž. Šmit and I. Orlić, Phys. Rev. A **50**, 1301 (1994).
[27] L. Sarkadi, T. Mukoyama, and Ž. Šmit, J. Phys. B **29**, 2253 (1996).
[28] H. C. Padhi, B. B. Dhal, T. Nandi, and D. Trautmann, J. Phys. B **28**, l59 (1995).
[29] L. Sarkadi, J. Phys. B **19**, L755 (1986).
[30] M. Pajek, A. P. Kobzev, R. Sandrik, R. A. Ilkhamov, and S. H. Khusmurodov, Nucl. Instrum. Methods Phys. Res. B **42**, 346 (1989).
[31] I. Orlić, J. Makjanić, G. H. J. Tros, and R. D. Vis, Nucl. Instrum. Methods Phys. Res. B **49**, 166 (1990).
[32] M. O. Krause, J. Phys. Chem. Ref. Data **8**, 307 (1979).
[33] P. Van Espen, K. Janssens, and J. Nobles, Chemom. Intell. Lab. Syst. **1**, 109 (1985).
[34] T. P. Thin and J. Leroux, X-Ray Spectrom. **8**, 85 (1979).
[35] J. F. Ziegler, J. P. Biersak, and U. Littmark, *The Stopping and Range of Ions in Solids* (Pergamon, New York, 1985) Vol. 1.
[36] M. Bozoian, K. M. Hubbard, and M. Nastasi, Nucl. Instrum. Methods Phys. Res. B **51**, 311 (1990).
[37] J. L'Ecuyer, J. A. Davies, and N. Matsunami, Nucl. Instrum. Methods **160**, 337 (1979).
[38] J. L. Campbell and J-X. Wang, At. Data Nucl. Data Tables **43**, 281 (1989).
[39] M. H. Chen, B. Crasemann, and H. Mark, Phys. Rev. A **24**, 177 (1981).
[40] T. J. Gray and N. B. Malhi, J. Phys. B **29**, 1331 (1996).
[41] H. L. Sun, J. L. Duggan, F. D. McDaniel, and G. Lapicki, Nucl. Instrum. Methods Phys. Res. B **99**, 192 (1995).
[42] U. Schiebel, T. J. Gray, R. K. Gardner, and P. Richard, J. Phys. B **10**, 2189 (1977).
[43] R. K. Gardner, T. J. Gray, P. Richard, C. Schmiedekamp, K. A. Jamison, and J. M. Hall, Phys. Rev. A **15**, 2202 (1979).
[44] R. J. Fortner, R. C. Der, T. M. Kavangh, and J. D. Garcia, J. Phys. B **5**, L73 (1972).
[45] C. Froese Fisher, Comput. Phys. Commun. **43**, 355 (1987).
[46] F. P. Larkins, J. Phys. B **4**, L29 (1971).